Paper:
De Jong, E., Williams, D., Abdelmohsen, L., Van Hest, J. & Zuhorn, I. (2018). A filter-free blood-brain barrier model to quantitatively study transendothelial delivery of nanoparticles by fluorescence spectroscopy. *Journal of Controlled Release, 289*, 14-22.
http://dx.doi.org/10.1016/j.jconrel.2018.09.015

Journal of Controlled Release 289 (2018) 14–22

Contents lists available at ScienceDirect

Journal of Controlled Release

journal homepage: www.elsevier.com/locate/jconrel

A filter-free blood-brain barrier model to quantitatively study transendothelial delivery of nanoparticles by fluorescence spectroscopy

Edwin De Jong[a], David S. Williams[b,c], Loai K.E.A. Abdelmohsen[b], Jan C.M. Van Hest[b], Inge S. Zuhorn[a,*]

[a] University of Groningen, University Medical Center Groningen, Department of Biomedical Engineering, Antonius Deusinglaan 1, 9713, AV, Groningen, the Netherlands
[b] Department of Biomedical Engineering, Department of Chemical Engineering and Chemistry, Eindhoven University of Technology, P.O. Box 513, 5600, MB, Eindhoven, the Netherlands
[c] Department of Chemistry, Swansea University, Swansea SA2 8PP, United Kingdom

ARTICLE INFO

Keywords:
Blood-brain barrier
Filter-free BBB model
Transcytosis
Polymersomes
G23 peptide

ABSTRACT

The delivery of therapeutics to the brain is greatly hampered by the blood-brain barrier (BBB). The use of nanoparticles that can cross the BBB via the process of receptor-mediated transcytosis at blood-brain barrier endothelial cells seems a promising strategy to transport therapeutics into the brain. To screen for suitable nanocarriers, and to study the process of transcytosis, a cultured polarized monolayer of brain microvascular endothelial cells on an extracellular matrix-coated porous membrane filter is widely used as an in vitro BBB model. However, due to the adhesion of numerous types of nanoparticles to the membrane filter and within the filter pores, such a model is unsuitable for the quantification of transendothelial delivery of nanoparticles. Hence, there is a pressing need for a filter-free in vitro BBB model. Ideally, the model is inexpensive and easy to use, in order to allow for its wide use in nanomedicine and biology laboratories around the world.

Here, we developed a filter-free in vitro BBB model that consists of a collagen gel covered with a monolayer of brain microvascular endothelial (hCMEC/D3) cells. The paracellular leakage of differently sized dextrans and the transcellular transport of LDL were measured to demonstrate the validity of the filter-free model. Finally, the transendothelial delivery of fluorescently-labelled PEG-P(CL-*g*-TMC) polymersomes that were functionalized with GM1-targeting peptides was assessed by fluorescence spectroscopy measurement of the luminal, cellular, and abluminal parts of the filter-free BBB model. Our data confirm the effectiveness of the G23 peptide to mediate transport of polymersomes across the BBB and the suitability of this filter-free in vitro model for quantification of nanoparticle transcytosis.

1. Introduction

The blood-brain barrier (BBB), which is formed by a polarized layer of brain capillary endothelial cells and supporting cell types [1], actively regulates the transport of substances between blood and brain. Adjacent endothelial cells are interconnected by tight junctions, thereby limiting the paracellular diffusion of macromolecules across the BBB [1]. Temporary disruption of tight junction integrity in order to enable passive drug diffusion through the BBB, or direct administration of a drug into the brain, e.g. via intracranial injection, are possible routes for drug delivery to the brain, but highly invasive [2]. Intravenous administration of drug-loaded nanoparticles decorated with moieties that promote their transendothelial transport into the brain, without compromising BBB integrity, is considered a less invasive alternative to treat brain diseases.

At the BBB the process of transcytosis in brain endothelial cells allows for the transcellular transport of specific endogenous macromolecules, providing a gateway for the delivery of nanoparticles into the brain [3–5]. The culture of a polarized monolayer of (human) brain microvascular endothelial cells on extracellular matrix (ECM)-coated porous membrane filters is widely used as an in vitro model for the BBB [6]. However, due to the adhesion of many types of nanoparticles to the membrane filter and within the filter pores, such a model is unsuitable for the reliable quantification of transendothelial delivery of nanoparticles [7,8]. Unfortunately, many of the recently developed microfluidic 'BBB-on-chip' systems do not provide a solution to this problem,

* Corresponding author at: University Medical Center Groningen, Department of Biomedical Engineering, Antonius Deusinglaan 1, 9713, AV, Groningen, the Netherlands.
E-mail address: i.zuhorn@umcg.nl (I.S. Zuhorn).

https://doi.org/10.1016/j.jconrel.2018.09.015
Received 25 April 2018; Received in revised form 15 September 2018; Accepted 18 September 2018
Available online 20 September 2018

because within these microfluidic systems similar membrane filters are used for cell support [9–15]. Furthermore, the recently developed filter-free BBB-on-chip systems, which consist of a microchannel that encloses a cylindrical ECM hydrogel with a lumen that is lined with human brain endothelium [16,17], are primarily useful for fluorescence microscopy studies. Lastly, the BBB-on-chip model designed by Adriani et al. [18] and the commercially available 3-lane OrganoPlate (Mimetas BV, the Netherlands) are systems that allow human brain endothelial cells to form a tubular monolayer against an ECM hydrogel (i.e. in the absence of an artificial membrane filter) and allow for access to the abluminal side of the endothelium. However, the surface area of the endothelial cell-ECM interface, which is $< 1\ mm^2$ in both systems, will limit the absolute amount of material transport across the BBB, while the diffusion of nanoparticles through the ECM hydrogel will be limited. Therefore, in these models, the quantification of nanoparticle transport across the BBB relies on the analysis of fluorescence microscopy images, or may necessitate the use of sensitive detection methods such as ELISA and mass spectrometry, which are time-consuming, expensive, and require expert knowledge.

Here, we set out to develop a filter-free in vitro BBB model for the quantification of transendothelial delivery of nanoparticles that is user-friendly and inexpensive. The model consists of a collagen gel in a conventional well plate covered with an hCMEC/D3 cell monolayer. A similar model was used by Gromnicova et al. to analyse the transport of gold nanoparticles across the barrier by transmission electron microscopy (TEM) [19,20]. However, electron microscopy is a labour intensive, time consuming and expensive technique that requires a high level of expertise [21–23]. Moreover, the detection of many types of organic nanoparticles, e.g. liposomes and polymersomes, within the complex cellular environment proves to be challenging with TEM [24]. Therefore, the model was redesigned in order to allow for the quantitative measurement of nanoparticle fluorescence in the apical, cellular and basolateral compartments by means of fluorescence spectroscopy.

In previous work we have demonstrated, both in vitro and in vivo, the transcytosis of non-biodegradable poly(ethylene glycol)-*block*-poly(butadiene) polymersomes decorated with the GM1-binding G23 peptide across the BBB [25,26]. The inability to biologically degrade polymersomes composed of these copolymers severely limits their application in drug delivery. Therefore, in this study, we developed biodegradable GM1-targeted polymersomes, consisting of poly(ethylene glycol)-*block*-poly(caprolactone-*gradient*-trimethylene carbonate) (PEG-P(CL-*g*-TMC)) copolymers, that are considered suitable for the actual delivery of drugs into the brain. In addition to the G23 peptide, we evaluated the transcytosis capacity of eight other GM1-binding peptides that were previously identified by phage display [25], demonstrating the suitability of our filter-free BBB model to quantify nanocarrier transcytosis.

2. Materials and methods

2.1. Cell culture

Human cerebral microvascular endothelial hCMEC/D3 cells were maintained in 25 cm^2 flasks precoated with 150 μg/ml rat tail collagen type-I (Enzo LifeSciences #ALX-522-435) in endothelial basal medium-2 (EBM-2) (Lonza #CC-3156) supplemented with 1 ng/ml human basic fibroblast growth factor (Peprotech #100-18B), 5 μg/ml ascorbic acid (Sigma-Aldrich #A4544), 1.4 μM hydrocortisone (Sigma-Aldrich #H0888), 10 mM HEPES (Gibco #15630-056), 1% (*v/v*) chemically defined lipid concentrate (Gibco #11905-031), 5% (*v/v*) foetal bovine serum (FBS), 100 units/ml of penicillin and 100 μg/ml streptomycin at 37 °C in a humidified atmosphere with 5% CO_2.

For experiments, hCMEC/D3 cells (passage 30–38) were seeded at a density of 1×10^5 cells/cm^2 onto collagen gels, with a gel volume of 450 μl per well, in a 24-wells plate (Corning #3524), and grown for five days in 1 ml of culture medium. The medium of hCMEC/D3 cells was replaced every other day. Collagen gels were prepared at a collagen concentration of 2 mg/ml by mixing 400 μl of the stock collagen solution (Enzo LifeSciences #ALX-522-435) with 100 μl of 10× phosphate-buffered saline (PBS), 490.8 μl of dH_2O and 9.2 μl of 1 M NaOH per ml of final collagen solution on ice, and incubated for 1 h at 37 °C in a humidified atmosphere to allow collagen gel formation.

2.2. Paracellular permeability assay

hCMEC/D3 cells were seeded onto collagen gels, and transwell filters (Corning #3401) precoated with 150 μg/ml rat tail collagen type-I. The cells were grown for five days and culture medium was replaced every other day. At day two to five, transwell-cultured hCMEC/D3 cells were washed once with prewarmed Hank's balanced salt solution (HBSS) (Gibco #14025) and 1 ml of prewarmed EBM-2 was added to the basolateral compartment of the transwell filter system. Subsequently, 500 μl of 1 mg/ml fluorescein isothiocyanate (FITC)-labelled dextran of 4 kDa (Sigma-Aldrich #FD-4) or 2000 kDa (Sigma-Aldrich #FD-2000S) in EBM-2 was added apically to the cells and incubated for 1 h at 37 °C. The medium from the basolateral compartment was collected immediately after the incubation period. Similarly, at day two to five, the hCMEC/D3 cultures on collagen gels were washed with HBSS and incubated with FITC-labelled dextran (4 kDa and 2000 kDa) for 1 h at 37 °C. After removal of the apical medium, the collagen gels with hCMEC/D3 cells were incubated with 200 μl 0.25% (*w/v*) collagenase A (Roche #10103578001) in HBSS for 90 min at 37 °C to solubilize the collagen. hCMEC/D3 cells were pelleted from this solution by centrifugation at 200 g for 5 min, and the supernatant, representing the basolateral compartment, was collected for quantification. The fluorescence intensity of the collected samples was measured using black flat-bottomed microplates (Greiner Bio-One #655209) and a Fluostar-Optima microplate reader (BMG Labtech) with excitation and emission at 485 nm and 520 nm, respectively. The quantity of dextran in the samples was determined using a standard curve of serially diluted FITC-labelled dextran. The apparent permeability was calculated according to the formula $P_{app} = (\Delta Q/\Delta t) \times (1/AC_0)$, where P_{app} is the apparent permeability coefficient (cm/min), $\Delta Q/\Delta t$ is the rate of permeation of dextran (μg/min) across the endothelial cell layer, A is the surface area of the cell layer (cm^2) and C_0 is the initial dextran concentration (μg/ml) applied to the apical cell surface.

2.3. Immunofluorescence microscopy

The hCMEC/D3 cell monolayers were washed once with prewarmed HBSS and fixed with 4% paraformaldehyde in PBS for 5 min. The cells were washed three times with PBS (pH 7.4) for 15 min and permeabilized with 0.2% Triton X-100 in PBS for 10 min. The cells were washed three times with PBS for 15 min before unspecific antibody binding was blocked by 5% goat serum (Vector Laboratories #S-1000) in PBS for 1 h. The cells were washed three times with PBS for 15 min and incubated with 5 μg/ml polyclonal rabbit anti-ZO-1 antibody (Invitrogen #61-7300) in 1% goat serum in PBS for 2 h at room temperature. The cells were washed 6 times with PBS for 15 min under gentle agitation before incubation with 4 μg/ml goat secondary antibody (Life Technologies #A-11034) and 1 μg/ml DAPI (Sigma-Aldrich #D9542) in 1% goat serum in PBS for 1 h at room temperature. The cells were washed 6 times with PBS for 15 min under gentle agitation. The collagen gels were removed from the 24-wells plate using a forceps and placed in aqueous mounting medium (DAKO #S3025) on a glass slide. The gels were covered with a coverslip and a Leica DM4000B fluorescence microscope (Leica Microsystems) was used to obtain fluorescence images, using 10× and 20× dry and 40× oil immersion objectives.

2.4. Lactate dehydrogenase assay

hCMEC/D3 cells were seeded at a density of 5×10^4 cells/cm^2 in a

96-wells plate (Corning #3599) precoated with 150 μg/ml rat tail collagen type-I and grown for five days in culture medium. The medium of the cells was replaced every other day. The cells were washed once with prewarmed HBSS, and subsequently treated with 50 μl of 0.25%, 0.5% and 1% (*w/v*) collagenase A in HBSS for 90 min at 37 °C. Spontaneous release of lactate dehydrogenase (LDH) by hCMEC/D3 cells was determined by incubation in HBSS alone. LDH activity was determined by measuring the absorbance at 490 nm in optically clear flat-bottomed microplates (Greiner Bio-One #655191) with a μQuant spectrophotometer (Bio-Tek Instruments) using a Cytotoxicity Detection Kit (Roche Diagnostics #11644793001) according to the manufacturer's protocol. Controls were included to correct for absorbance caused by collagenase A and interference of collagenase A with LDH activity. The percentage of LDH release as induced by incubation of hCMEC/D3 cells with collagenase A was expressed relative to the maximum LDH release by the hCMEC/D3 cells.

2.5. Fluorescent labelling of low density lipoprotein

Human low density lipoprotein (LDL) (Calbiochem #437644) was diluted in 100 mM sodium bicarbonate buffer (pH 9) to a protein concentration of 2 mg/ml and FITC (Sigma-Aldrich #F7250) was dissolved in DMSO at a concentration of 2 mg/ml. 5 mg of LDL, which corresponds to 1 mg of protein content, and 15 μg of FITC were mixed and incubated for 2 h at room temperature. Unbound FITC was removed by dialysis against sterile PBS (pH 7.4) with two buffer changes over a 24-h period using a 10 kDa molecular weight cut-off dialysis cassette (Thermo Scientific #66380). The protein concentration of fluorescently-labelled LDL was determined by measuring the absorbance at 750 nm in an optically clear flat-bottomed microplate (Greiner Bio-One #655191) with a μQuant spectrophotometer (Bio-Tek Instruments) using the DC protein assay kit (Bio-Rad #500-0112) according to the manufacturer's protocol. LDL was diluted to a concentration of 2 mg/ml in PBS (corresponding to 400 μg protein/ml) and stored at 4 °C.

2.6. Assembly of PEG-P(CL-g-TMC) polymersomes

Amphiphilic block copolymers were produced as previously described [27]. Polymersomes, composed of poly(ethylene glycol)$_{22}$-*block*-poly(caprolactone$_{28}$-*gradient*-trimethylene carbonate$_{31}$) (PEG$_{22}$-P(CL$_{28}$-*g*-TMC$_{31}$)), nitrobenzoxadiazole-labelled poly(ethylene glycol)$_{22}$-*block*-poly(caprolactone$_{28}$-*gradient*-trimethylene carbonate$_{31}$) (NBD-PEG$_{22}$-P(CL$_{28}$-*g*-TMC$_{31}$)) and maleimide-functionalized poly(ethylene glycol)$_{75}$-*block*-poly(caprolactone$_{28}$-*gradient*-trimethylene carbonate$_{31}$) (MAL-PEG$_{75}$-P(CL$_{28}$-*g*-TMC$_{31}$)) copolymers were assembled through the direct hydration method. The different PEG chain length for the maleimide-functionalized copolymer was chosen to ensure a good display of the targeting moieties on the surface of the polymersomes. The PEG$_{22}$-P(CL$_{28}$-*g*-TMC$_{31}$), NBD-PEG$_{22}$-P(CL$_{28}$-*g*-TMC$_{31}$) and MAL-PEG$_{75}$-P(CL$_{28}$-*g*-TMC$_{31}$) copolymers were dissolved at 10 wt% in poly (ethylene glycol) methyl ether (350) (Fluka #81318) at 60 °C and mixed at a molar ratio of 94:4:2. After the copolymer solution was cooled to room temperature, 150 and 300 μl of PBS (pH 7.4) were added to 4 mg of copolymer and magnetically stirred at 200 rpm for 5 min after each addition. The polymersome emulsion was extruded 11 times over a 100 nm polycarbonate filter.

2.7. Conjugation of peptides to polymersomes

Peptides were synthesized by JPT Peptide Technologies (Berlin, Germany) with a purity of over 90% as analysed by HPLC and mass spectrometry. The addition of an amidated C-terminal cysteine residue to the native peptide sequences allowed for their conjugation to the polymersomes via a maleimide-thiol reaction. 200 μg of peptide lyophilisate was dissolved in 50 μl of 10 mM acetic acid, and subsequently mixed with 50 μl PBS (pH 7.4). The concentration of peptides was determined by measuring the absorbance at 280 nm with the Nanodrop One spectrophotometer (Thermo Scientific). A 2-fold molar excess of peptide relative to MAL-PEG$_{75}$-P(CL$_{28}$-*g*-TMC$_{31}$) copolymer was added to the polymersomes and the conjugation reaction was allowed to proceed for 2 h at room temperature. The polymersomes were diluted to a concentration of 2 mg/ml by the addition of PBS. Non-coupled peptide was removed by dialysis against sterile PBS with two buffer changes over a 24-h period using a 10 kDa molecular weight cut-off dialysis cassette (Thermo Scientific #66380) at 4 °C. The polymersomes were diluted to a concentration of 1 mg/ml in PBS and stored at 4 °C. Prior to the assembly of non-functionalized PEG-P(CL-*g*-TMC) polymersomes, the maleimide-functionalized copolymer was reacted with ethanethiol to block the maleimide residues.

2.8. Characterization of the polymersomes

Size, polydispersity, and ζ-potential of the polymersomes were determined at a temperature of 25 °C with a Zetasizer Nano ZS particle analyser (Malvern Instruments) using a standard 633 nm laser. The polymersomes were diluted in 10 mM NaCl to a concentration of 100 μg/ml, and subsequently loaded into a folded capillary cell (Malvern Instruments #DTS1070). Dynamic light scattering measurements were performed in triplicate with a backscattering detection angle of 173°. Size and polydispersity were calculated by the cumulant analysis method using Zetasizer software version 7.10. The ζ-potential was determined by measuring the electrophoretic mobility and calculated using the Smoluchowski approximation.

The morphology of the G23-PEG-P(CL-*g*-TMC) polymersomes was imaged using a 300 kV FEI Titan transmission electron cryo-microscope (FEI Company) equipped with a LaB6 filament and an autoloader station. Lacey carbon coated 200 mesh copper grids (Electron Microscopy Sciences) were treated in the Cressington 208 carbon coater (Cressington Scientific Instruments) for 40 s, and subsequently 3 μl of a 2 mg/ml polymersome emulsion was applied to the plasma treated grid. The grid was blotted for 3 s with an offset of -3 at 100% humidity using the Vitrobot Mark III (FEI Company) and directly frozen in vitreous ice by plunging into liquid ethane.

2.9. Transcytosis assay

hCMEC/D3 cell monolayers were washed once with prewarmed HBSS. Subsequently, 500 μl of FITC-labelled LDL (100 μg/ml and 200 μg/ml) diluted in EBM-2 or 100 μg/ml NBD-labelled polymersomes diluted in EBM-2 + 5% FBS was added apically to the cells and incubated at 37 °C for 2 and 4 h, or 4, 8 and 16 h, respectively. After the incubation period, the medium was collected and the cells were washed with 500 μl prewarmed HBSS to collect residual LDL or polymersomes (total volume of apical fraction: 1 ml). The collagen gels were digested in 200 μl 0.25% (*w/v*) collagenase A (Roche #10103578001) in HBSS for 90 min at 37 °C. The cells were pelleted by centrifugation at 200 *g* for 5 min. The supernatant was collected and mixed with 400 μl EBM-2 or EBM-2 + 5% FBS (total volume of basolateral fraction: 1 ml). The hCMEC/D3 cell pellet was soaked in 500 μl of ultrapure water for 10 min, and subsequently mixed with 500 μl of EBM-2 or EBM-2 + 5% FBS (total volume of cellular fraction: 1 ml). The fluorescence intensities in the apical, cellular, and basolateral fractions were measured in triplicate using black flat-bottomed microplates (Greiner Bio-One #655209) and a Fluostar-Optima microplate reader (BMG Labtech) with excitation and emission at 485 nm and 520 nm, respectively. The fluorescence in the distinct apical, cellular, and basolateral fractions without LDL or polymersomes, i.e. background fluorescence, was subtracted from the measured intensity values. The percentage of LDL or polymersomes fluorescence associated with the apical, cellular and basolateral fraction was expressed relative to the total fluorescent content present in all three fractions collectively. The percentage of total recovery was calculated from the ratio between the total

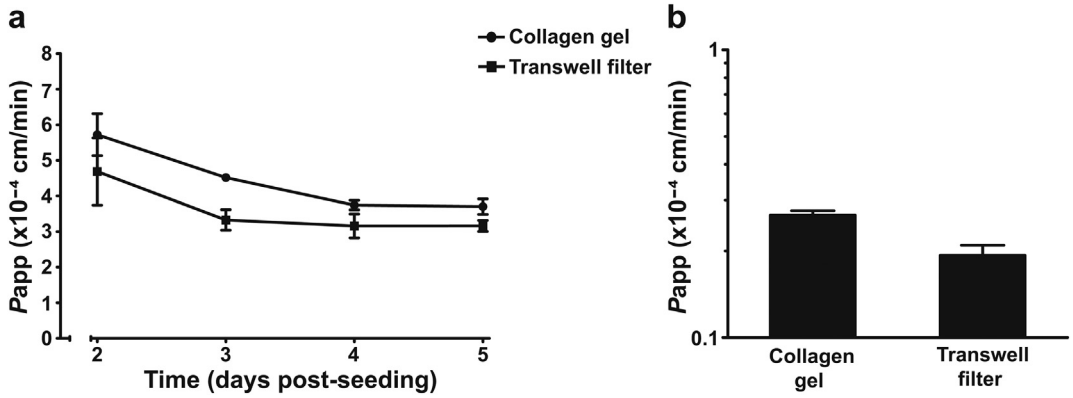

Fig. 1. Paracellular permeabilities for dextrans in brain endothelial cell monolayers grown on collagen gels or transwell filters. Fluorescently-labelled dextrans were added apically to the cell monolayers and incubated for 1 h at 37 °C. The quantity of dextran in the basolateral collagen gel fraction or transwell filter compartment was used to calculate the apparent permeability coefficients (P_{app}). (a) P_{app} for 4 kDa dextran in hCMEC/D3 cell cultures at two to five days post-seeding. (b) P_{app} for 2000 kDa dextran in hCMEC/D3 cell monolayers five days post-seeding. Each value represents the mean ± S.D. of three independent experiments performed in duplicate.

fluorescent content measured in all three fractions and the fluorescence of the LDL or polymersome solution that was added apically at the onset of the assay. The percentages of total recovery were > 85%.

3. Results and discussion

3.1. hCMEC/D3 monolayer tightness is similar in the filter-free and transwell BBB model

In order to assess the tightness of the hCMEC/D3 monolayer in our filter-free BBB model, the apparent permeability coefficients (P_{app}) for 4 kDa and 2000 kDa dextran were determined, and compared to the P_{app} in the conventional transwell BBB model. As shown in Fig. 1, the paracellular permeability of the conventional BBB model for dextran of 4 kDa decreased up to four days post-seeding and reached a P_{app} of $3.16 \pm 0.15 \times 10^{-4}$ cm/min at five days post-seeding (Fig. 1a). The filter-free BBB model showed a similar increase in barrier formation in time for 4 kDa dextran and demonstrated a P_{app} of $3.70 \pm 0.22 \times 10^{-4}$ cm/min at day five post-seeding (Fig. 1a), indicating the formation of a confluent hCMEC/D3 cell monolayer on collagen gel within four to five days post-seeding. This P_{app} value corresponds to the P_{app} values that were determined for two other filter-free 3D BBB-on-a-chip models using fluorescence microscopy [16,17]. For dextran of 2000 kDa the filter-free and the conventional BBB model demonstrated a decrease in paracellular permeability of an order of a magnitude compared to 4 kDa dextran, resulting in a P_{app} of $0.27 \pm 0.01 \times 10^{-4}$ and $0.19 \pm 0.02 \times 10^{-4}$ cm/min (Fig. 1b), respectively. These P_{app} values correspond to a > 99% block of 2000 kDa dextran passage across the BBB for both in vitro BBB models. The size-dependent permeability for dextrans indicates the integrity of the endothelial cell monolayer on collagen gel in the filter-free BBB model.

Tight junctions between adjacent endothelial cells limit the paracellular diffusion of macromolecules, including dextrans, across the BBB. To further confirm monolayer integrity in the filter-free BBB model, the expression of the tight junction protein zonula occludens-1 (ZO-1) was assessed in hCMEC/D3 cell monolayers grown on collagen gel by immunofluorescence microscopy. ZO-1 showed a continuous staining pattern at the lateral membranes of neighbouring brain endothelial cells (Fig. 2), which confirms the formation of a continuous hCMEC/D3 cell monolayer grown on a collagen gel.

3.2. hCMEC/D3 cells maintain cell membrane integrity during Collagenase A digestion of the collagen gel in the filter-free BBB model

In order to collect the cellular and basolateral fractions in the filter-free BBB model, the apical medium was aspirated and the collagen gel containing the hCMEC/D3 monolayer was digested with collagenase A. Following collagenase A treatment the resulting suspension was centrifuged to separate the cells (pellet) from the basolateral (supernatant) fraction. To exclude the possibility of passive leakage of material from the cellular interior into the basolateral fraction, because of collagenase A-induced plasma membrane damage in the endothelial cells, the release of lactate dehydrogenase (LDH) from the endothelial cells upon incubation with collagenase A was tested. hCMEC/D3 cells were treated with various concentrations of collagenase A for 90 min at 37 °C. Collagenase A at a concentration up to 0.5% (*w/v*), which is twice the concentration that is used for digestion of the collagen gel in our assay, did not significantly increase the release of LDH compared to the spontaneous LDH release by endothelial cells (Fig. 3). These data demonstrate that collagenase A at a concentration of 0.25% (*w/v*) allows for the digestion of the collagen gel without damaging the endothelial plasma membrane.

3.3. Quantitative measurement of low density lipoprotein transport across the filter-free BBB model

Transport of low density lipoprotein (LDL) across the BBB occurs through the process of transcytosis [28,29]. Therefore, to establish the capacity of hCMEC/D3 cell monolayers grown on collagen gels for active transport through transcytosis, the transendothelial transport of LDL was quantitatively studied by fluorescence spectroscopy. Fluorescently-labelled LDL at a quantity of 50 and 100 μg was apically added to hCMEC/D3 cell monolayers and incubated for 2 and 4 h at 37 °C. The apical addition of 50 μg of LDL demonstrated a basolateral recovery of 12.4 ± 2.0% and 17.6 ± 1.5% after 2 and 4 h of incubation (Fig. 4a), respectively. A similar transcytosis efficiency was observed with 100 μg of LDL, i.e. a basolateral recovery of 12.8 ± 2.3% and 17.9 ± 1.5% after 2 and 4 h of incubation (Fig. 4b), respectively. The barrier integrity of the endothelial cell monolayer was not compromised by the presence of LDL, as was shown by an unaltered paracellular permeability for 4 kDa dextran compared to cells without LDL (data not shown). This means that incubation of cells with LDL does not result in an increased transport of LDL via the paracellular route. Since the transcellular transport of macromolecules is a temperature-dependent process, the basolateral recovery of fluorescently-labelled LDL was examined after incubation at 4 °C and compared to the recovery after incubation at 37 °C. A significant decrease in basolateral recovery of LDL was observed after incubation at low temperature (19.5 ± 0.2% at 37 °C compared to 7.4 ± 0.4% at 4 °C), i.e. a > 2.5-fold decrease. This indicates that LDL requires active mechanisms for transport across the

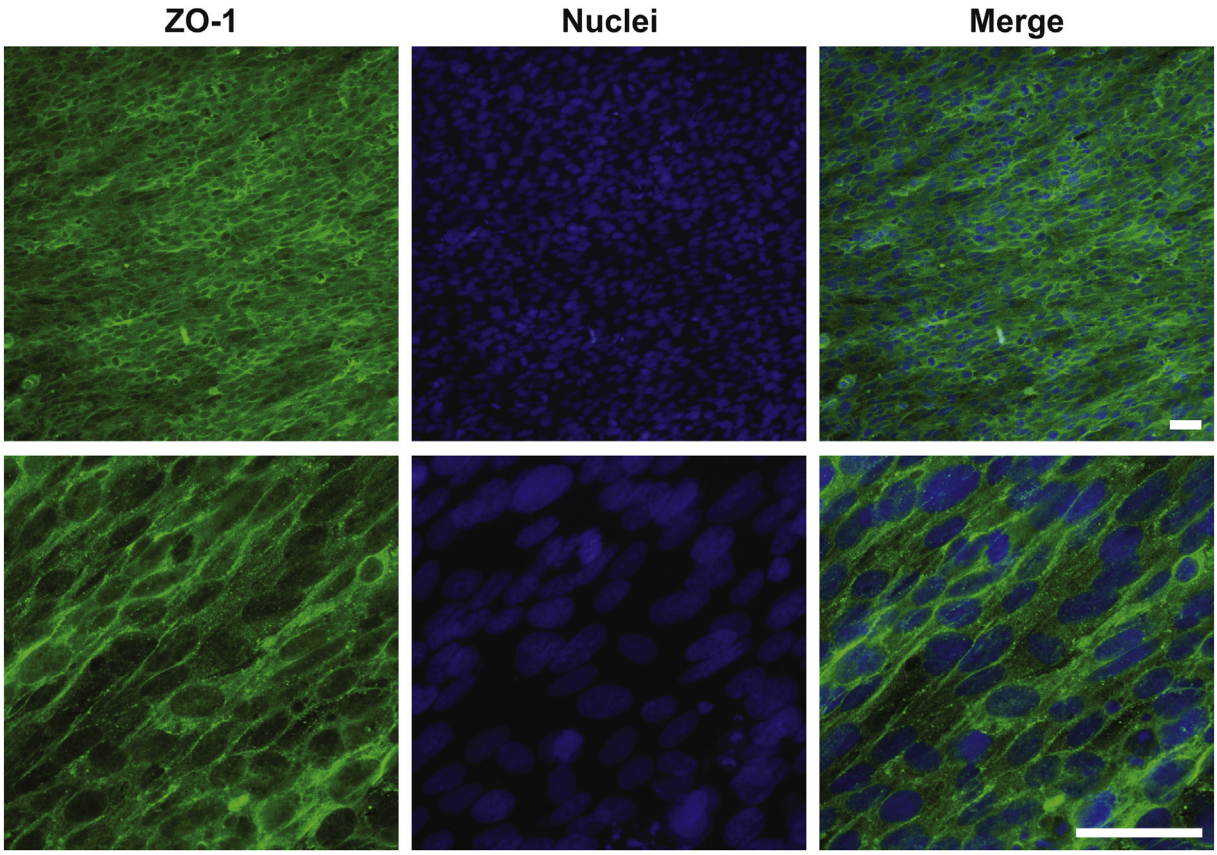

Fig. 2. Expression of the tight junction protein zonula occludens-1 (ZO-1) in hCMEC/D3 cells grown on collagen gels. hCMEC/D3 cell monolayers grown on collagen gels were immunostained for ZO-1 (green). Cell nuclei were stained with DAPI (blue). Scale bars represent 50 μm. (For interpretation of the references to colour in this figure legend, the reader is referred to the web version of this article.)

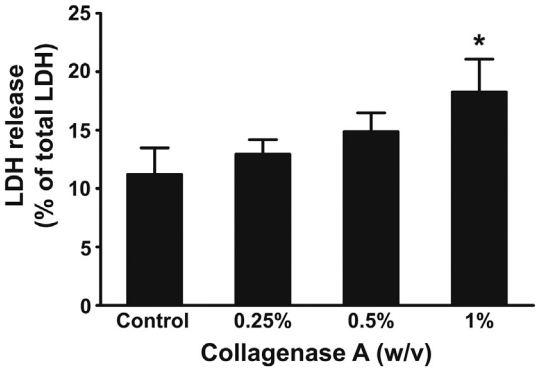

Fig. 3. Lactate dehydrogenase (LDH) release from brain endothelial cells treated with various concentrations of collagenase A. hCMEC/D3 cells grown in a 96-wells plate were treated with 0.25%, 0.5% and 1% (*w/v*) collagenase A in HBSS for 90 min and activity of the LDH released by the cells was determined. Each value represents the mean ± S.D. of three independent experiments performed in triplicate. Data were analysed by one-way ANOVA followed by a Dunnett post hoc test and considered significantly different from the control for a *p* value lower than 0.05 (*).

BBB model, but does not exclude a contribution of paracellular transport. Because a relatively low junctional tightness has been described for hCMEC/D3 cell monolayers [30], the paracellular leakage of 250 kDa dextran, a small molecule with a similar size as LDL (20-25 nm; [31]) was investigated next. Apical addition of 100 μg 250 kDa dextran to the filter-free BBB model demonstrated a basolateral recovery of 1.7 ± 0.1% after 1 h at 37 °C (data not shown). Assuming a linear curve for paracellular transport in time, 1.7% basal recovery after 1 h would give 6.8% after 4 h, which is similar to the 7.4% that was detected for passive LDL transport at 4 °C. Finally, the possibility of active LDL excretion by the endothelial cells during collagenase A digestion was excluded. Namely, the amount of LDL that was found in the cellular fraction following collagenase A digestion at 37 °C was similar to the amount that was detected after digestion at 4 °C (data not shown), indicating that LDL is not actively exported from the cells during collagenase A treatment. Altogether, the data indicate that the filter-free BBB model allows for the quantitative assessment of active and passive LDL transport following collection of the apical, cellular, and basolateral fractions by means of collagenase A digestion.

3.4. Quantitative measurement of the transport of G23-PEG-P(CL-g-TMC) polymersomes across the filter-free BBB model

In contrast to the non-biodegradable GM1-targeted poly(ethylene glycol)-*block*-poly(butadiene) polymersomes [25], the G23-PEG-P(CL-*g*-TMC) polymersomes were not able to cross the membrane filter of a transwell system. Therefore, the filter-free BBB model was necessary in order to quantitatively study the transcytosis of nanoparticles, including polymersomes. Biodegradable polymersomes composed of 94 mol% of PEG_{22}-P(CL_{28}-*g*-TMC_{31}) copolymer, 4 mol% of fluorescently-labelled PEG_{22}-P(CL_{28}-*g*-TMC_{31}) and 2 mol% of maleimide-functionalized PEG_{75}-P(CL_{28}-*g*-TMC_{31}) copolymer were made using the direct hydration method, while functionalization with cysteine-terminated GM1-targeting peptides was performed via a maleimide-thiol reaction (see Materials and methods). Conjugation of the G23 peptide to the PEG-P(CL-*g*-TMC) polymersomes resulted in a negligible shift in their mean size and polydispersity from 123 to 138 nm and 0.11 to 0.23 (Table 1), respectively. Also, the ζ-potential remained similarly negative after peptide conjugation to the polymersomes (Table 1). Finally,

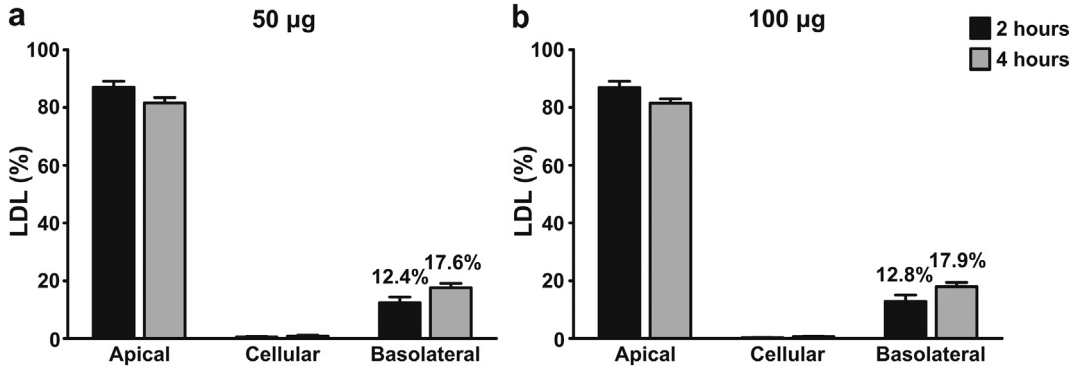

Fig. 4. Transcytosis of low density lipoprotein (LDL) in the filter-free BBB model. Fluorescently-labelled LDL at a quantity of 50 (a) and 100 µg (b) was added apically to the cells and incubated for 2 and 4 h at 37 °C. The percentage of LDL associated with the apical, cellular and basolateral fraction is expressed relative to the total fluorescent content present in all three fractions collectively. Each value represents the mean ± S.D. of three independent experiments performed in duplicate.

the morphology of the G23-PEG-P(CL-*g*-TMC) polymersome formulation was examined by cryo-TEM. Spherical bilayer structures, i.e. polymersomes with a size > 50 nm were identified (Fig. 5). Asymmetric flow field flow fractionation (AF4) in combination with dynamic light scattering (DLS) indicated the presence of polymersomes with an average size of 100 nm, and a neglectable amount (< 1%) of micellar structures (data not shown).

Next, the transcytosis capacity of the G23-PEG-P(CL-*g*-TMC) polymersomes was analysed using the filter-free BBB model and fluorescence spectroscopy. Fluorescently-labelled polymersomes were added apically to the cells and incubated for 4, 8 and 16 h at 37 °C. After 4 h of incubation, the hCMEC/D3 cell monolayer showed an uptake of 5.0 ± 3.4% of G23-PEG-P(CL-*g*-TMC) polymersomes, whereas the internalization of non-functionalized (control) PEG-P(CL-*g*-TMC) polymersomes was 0.6 ± 0.4% (Fig. 6a). Moreover, 4.8 ± 2.2% of G23-PEG-P(CL-*g*-TMC) polymersomes and 1.2 ± 0.3% of control polymersomes accumulated at the basolateral side of the BBB (Fig. 6a). Hence, the G23 peptide mediated a 4-fold increase in the transcytosis capacity of polymersomes after 4 h of incubation. Prolonged incubation of the filter-free BBB model with PEG-P(CL-*g*-TMC) polymersomes for 8 h and 16 h did not result in an increase in cellular uptake and/or basolateral accumulation (Fig. 6b and c). In contrast, the basolateral accumulation of G23-PEG-P(CL-*g*-TMC) polymersomes increased to 6.6 ± 2.2% and 6.5 ± 2.3% after 8 and 16 h of incubation (Fig. 6b and c), respectively, demonstrating a ~7-fold increase in the transcytosis capacity of G23-PEG-P(CL-*g*-TMC) polymersomes compared to control polymersomes. Importantly, incubation of the hCMEC/D3 cell monolayer with and without G23-PEG-P(CL-*g*-TMC) polymersomes showed equal levels of paracellular permeability for 4 kDa dextran, indicating that the barrier integrity of the endothelial cell monolayer was not compromised by the presence of G23-PEG-P(CL-*g*-TMC) polymersomes (data not shown). Overall, the data exclude the involvement of paracellular transport of G23-PEG-P(CL-*g*-TMC) polymersomes across the BBB, specifying the involvement of active transcellular transport, i.e. transcytosis, in the passage of G23-PEG-P(CL-*g*-TMC) polymersomes across the filter-free BBB model. The association of (G23-)PEG-P(CL-*g*-TMC) polymersomes with hCMEC/D3 cell monolayers grown on collagen gels was demonstrated by fluorescence microscopy (Fig. 7), confirming the increase in cellular association after conjugation of the G23 peptide to the

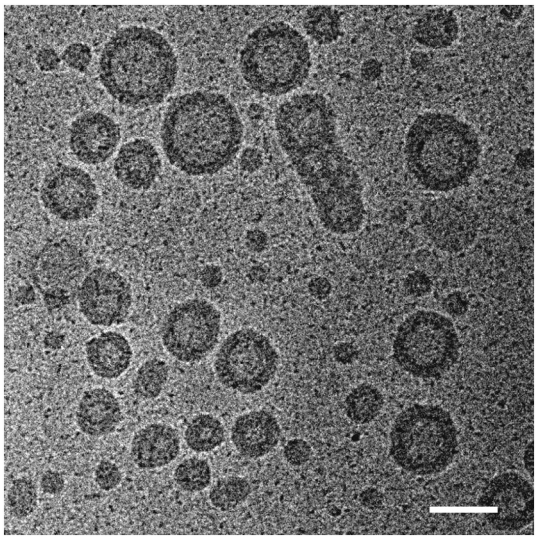

Fig. 5. Morphological examination of G23-PEG-P(CL-*g*-TMC) polymersomes by cryo-TEM. G23-PEG-P(CL-*g*-TMC) polymersomes examined by cryo-TEM revealed spherical bilayer structures with a size > 50 nm. Scale bar represents 100 nm.

Table 1
Physical characterization of the PEG-P(CL-*g*-TMC) polymersomes conjugated to the different GM1-targeting peptide sequences. Mean diameter, polydispersity (PDI), and ζ-potential of the polymersomes functionalized with GM1-targeting peptides was measured using a particle analyser. Each value represents the mean ± S.D. of two different batches of polymersomes.

Polymersomes	Peptide sequence	Size (nm)	PDI	ζ-potential (mV)
PEG-P(CL-*g*-TMC)	–	123 ± 3.1	0.11 ± 0.01	−5.9 ± 0.4
G23-PEG-P(CL-*g*-TMC)	H-HLNILSTLWKYRC-NH2	138 ± 0.2	0.23 ± 0.07	−4.4 ± 0.1
G2-PEG-P(CL-*g*-TMC)	H-HSSWWLALAKPTC-NH2	134 ± 4.5	0.26 ± 0.03	−6.4 ± 0.3
G18-PEG-P(CL-*g*-TMC)	H-HTKQIPRHIYSAC-NH2	145 ± 7.9	0.17 ± 0.03	−4.9 ± 0.1
G29-PEG-P(CL-*g*-TMC)	H-MPAVMSSAQVPRC-NH2	127 ± 3.5	0.11 ± 0.01	−4.1 ± 0.8
G32-PEG-P(CL-*g*-TMC)	H-YQLRPNAESLRFC-NH2	130 ± 6.2	0.14 ± 0.06	−5.2 ± 0.5
G47-PEG-P(CL-*g*-TMC)	H-YSNTLPLNLPPYC-NH2	128 ± 3.4	0.11 ± 0.01	−6.9 ± 0.2
G88-PEG-P(CL-*g*-TMC)	H-NPAGPSPAHIISC-NH2	126 ± 3.0	0.10 ± 0.01	−5.4 ± 0.4
G92-PEG-P(CL-*g*-TMC)	H-HSSWYIQHFPPLC-NH2	135 ± 0.1	0.18 ± 0.01	−7.4 ± 0.6
G117-PEG-P(CL-*g*-TMC)	H-LLADTTHHRPWTC-NH2	126 ± 2.9	0.09 ± 0.01	−5.2 ± 1.0

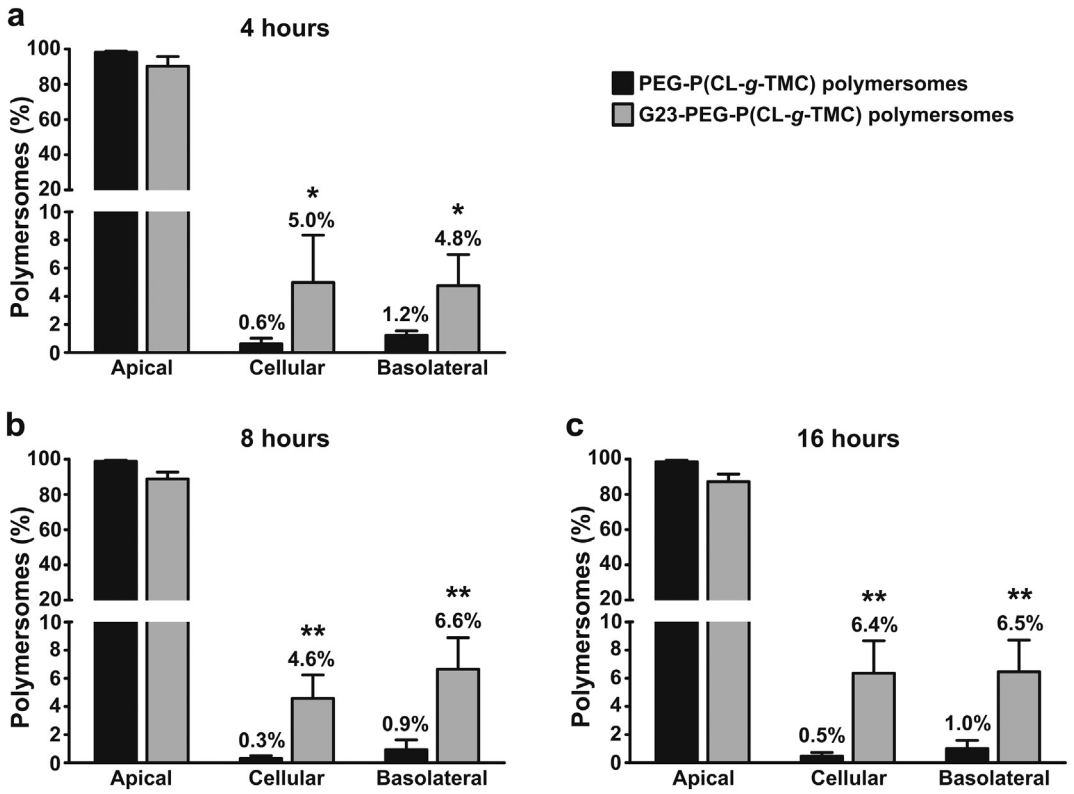

Fig. 6. Transcytosis of G23-PEG-P(CL-*g*-TMC) polymersomes in the filter-free BBB model. Fluorescently-labelled polymersomes at a quantity of 50 μg were added apically to the cells and incubated for 4 (a), 8 (b) and 16 (c) hours at 37 °C. The percentage of polymersomes associated with the apical, cellular and basolateral fraction is expressed relative to the total fluorescent content present in all three fractions collectively. Each value represents the mean ± S.D. of four independent experiments performed in duplicate. Data were analysed by Student *t*-test and statistically significant differences between polymersomes with and without the G23 peptide are indicated with (*) for a *p* value lower than 0.05 and (**) for a *p* value lower than 0.005.

polymersomes.

3.5. Quantitative measurement of the transcytosis capacity of PEG-P(CL-g-TMC) polymersomes functionalized with GM1-binding peptides using the filter-free BBB model

In order to assess the transcytosis capacity of the GM1-targeting peptide sequences obtained from our earlier phage library screening [25], biodegradable PEG-P(CL-*g*-TMC) polymersomes were functionalized with the different peptides G2, G18, G29, G32, G47, G88, G92, and G117 and their transcytosis was measured using the newly developed filter-free BBB model. Conjugation of the different GM1-targeting peptides to the biodegradable polymersomes resulted in a minimal shift in their mean size and ζ-potential (Table 1), excluding a potential effect of differences in size and charge of the functionalized polymersomes on their cellular processing. Functionalization of the polymersomes with the different GM1-targeting peptides, however, did neither increase their cellular internalization nor their transcytosis across the filter-free BBB model compared to non-functionalized polymersomes (Fig. 8). Apparently, only the G23 peptide is able to mediate transcytosis of polymersomes across the BBB, like shown previously with non-biodegradable poly(ethylene glycol)-*block*-poly(butadiene) polymersomes [25].

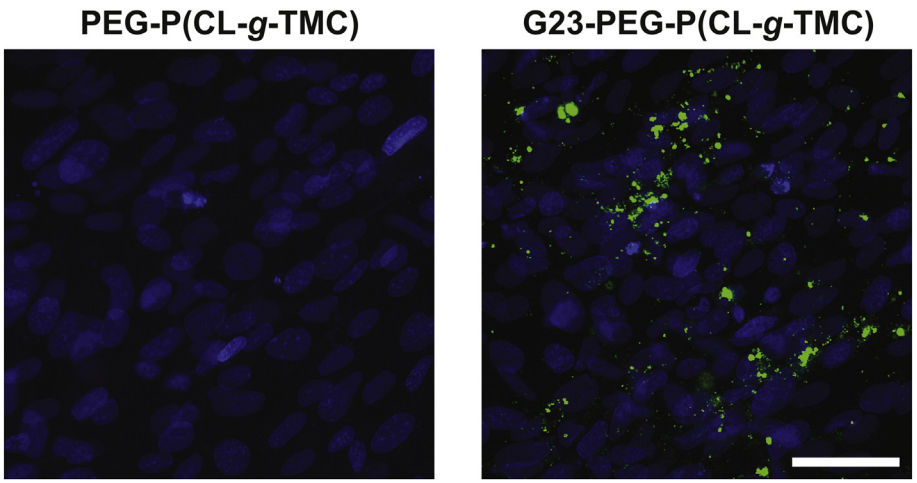

Fig. 7. Enhanced association of G23-PEG-P(CL-*g*-TMC) polymersomes compared to PEG-P(CL-*g*-TMC) polymersomes with hCMEC/D3 cell monolayers grown on collagen gels. Fluorescently-labelled polymersomes (green) at a quantity of 50 μg were added apically to the cells and incubated for 8 h at 37 °C. Cell nuclei were stained with DAPI (blue). Scale bar represents 50 μm. (For interpretation of the references to colour in this figure legend, the reader is referred to the web version of this article.)

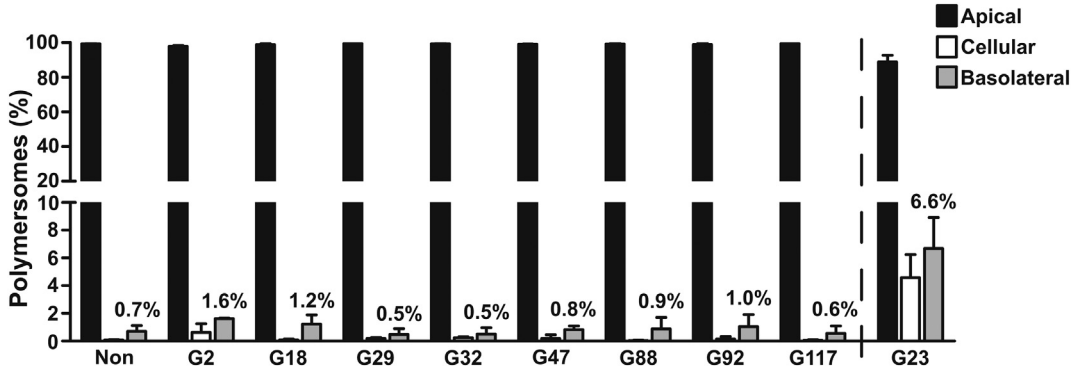

Fig. 8. Transcytosis of GM1-targeted PEG-P(CL-*g*-TMC) polymersomes in the filter-free BBB model. Fluorescently-labelled polymersomes at a quantity of 50 μg were added apically to the cells and incubated for 8 h at 37 °C. The percentage of polymersomes associated with the apical, cellular and basolateral fraction is expressed relative to the total fluorescent content present in all three fractions collectively. Each value represents the mean ± S.D. of four independent experiments performed in duplicate. The data for G23-PEG-P(CL-*g*-TMC) polymersomes from Fig. 6b were included for ease of comparison.

4. Conclusions

In the present study, we have successfully established a filter-free in vitro BBB model that allows for high throughput quantitative measurement of transendothelial transport of nanocarriers by fluorescence spectroscopy. Using this model, the transcytotic potential of GM1-targeted biodegradable polymersomes was determined. G23-PEG-P(CL-*g*-TMC) polymersomes showed 6.6 ± 2.2% transcytosis following 8 h of incubation and will be further developed to transport drugs across the BBB in order to treat brain diseases. Since there is no membrane filter involved in the presented BBB model, the transendothelial transport of drug-loaded nanoparticles decorated with moieties that promote transcytosis across the BBB now can be evaluated in a setting that more closely mimics the in vivo situation. Furthermore, in order to quantitatively study the transport of nanoparticles across other cellular barriers of the human body, the same setup can be used to create filter-free barrier models with the use of relevant primary or immortalized endothelial or epithelial cells cultured on extracellular matrix (ECM) gels. Next to the quantification of cellular uptake and transcytosis of nanoparticles, filter-free models will prove useful for mechanistic studies. Here, fast live cell imaging techniques, including total internal reflection fluorescence (TIRF), are useful, especially to study cellular dynamics, while (immuno)electron microscopic investigation allows for the determination of subcellular details, including barrier integrity. A limitation of the presented filter-free BBB model is its use in combination with (fluorescence) microscopy at high magnification. Since the collagen gel is > 2 mm in height and is prepared in a conventional well plate, the limited working distance of high magnification objectives hampers image acquisition. This problem can be solved by fixation of the cells and collagen gel, and subsequent positioning of the specimen between a glass slide and a coverslip, as described. However, without fixation of the gels, it proved difficult to transfer the collagen gel with cells while maintaining cell monolayer integrity. Therefore, for high magnification imaging using (fluorescence) microscopy, we recommend to use ECM-coated coverslips.

Acknowledgements

This work was supported by the Dutch Technology Foundation STW (which is part of the Netherlands Organisation for Scientific Research (NWO), and which is partly funded by the Ministry of Economic Affairs, Netherlands) and the Dutch Ministry of Education, Culture and Science (Gravitation program 024.001.035).

Additional information

The authors declare that they have no conflicts of interest.

References

[1] B.W. Chow, C. Gu, The molecular constituents of the blood-brain barrier, Trends Neurosci. 38 (10) (2015) 598–608.
[2] C.T. Lu, Y.Z. Zhao, H.L. Wong, J. Cai, L. Peng, X.Q. Tian, Current approaches to enhance CNS delivery of drugs across the brain barriers, Int. J. Nanomedicine 9 (2014) 2241–2257.
[3] F. Fang, D. Zou, W. Wang, Y. Yin, T. Yin, S. Hao, B. Wang, G. Wang, Y. Wang, Non-invasive approaches for drug delivery to the brain based on the receptor mediated transport, Mater. Sci. Eng. C Mater. Biol. Appl. 76 (2017) 1316–1327.
[4] A.M. Grabrucker, B. Ruozi, D. Belletti, F. Pederzoli, F. Forni, M.A. Vandelli, G. Tosi, Nanoparticle transport across the blood brain barrier, Tissue Barriers. 4 (1) (2016) e1153568.
[5] J.V. Georgieva, D. Hoekstra, I.S. Zuhorn, Smuggling drugs into the brain: an overview of ligands targeting transcytosis of drug delivery across the blood-brain barrier, Pharmaceutics. 6 (4) (2014) 557–583.
[6] H.C. Helms, N.J. Abbott, M. Burek, R. Cecchelli, P.O. Couraud, M.A. Deli, C. Förster, H.J. Galla, I.A. Romero, E.V. Shusta, M.J. Stebbins, E. Vandenhaute, B. Weksler, B. Brodin, In vitro models of the blood-brain barrier: an overview of the commonly used brain endothelial cell culture models and guidelines for their use, J. Cereb. Blood Flow Metab. 36 (5) (2016) 862–890.
[7] D. Ye, M.N. Raghnaill, M. Bramini, E. Mahon, C. Åberg, A. Salvati, K.A. Dawson, Nanoparticle accumulation and transcytosis in brain endothelial cell layers, Nanoscale 5 (22) (2013) 11153–11165.
[8] L. Cartwright, M.S. Poulsen, H.M. Nielsen, G. Pojana, L.E. Knudsen, M. Saunders, E. Rytting, In vitro placental model optimization for nanoparticle transport studies, Int. J. Nanomedicine 7 (2012) 497–510.
[9] Y.I. Wang, H.E. Abaci, M.L. Shuler, Microfluidic blood-brain barrier model provides in vivo-like barrier properties for drug permeability screening, Biotechnol. Bioeng. 114 (1) (2017) 184–194.
[10] M.W. Van Der Helm, M. Odijk, J.P. Frimat, A.D. Van Der Meer, J.C. Eijkel, A. Van Den Berg, L.I. Segerink, Direct quantification of transendothelial electrical resistance in organs-on-chips, Biosens. Bioelectron. 85 (2016) 924–929.
[11] O. Kilic, D. Pamies, E. Lavell, P. Schiapparelli, Y. Feng, T. Hartung, A. Bal-Price, H.T. Hogberg, A. Quinones-Hinojosa, H. Guerrero-Cazares, A. Levchenko, Brain-on-chip model enables analysis of human neural differentiation and chemotaxis, Lab Chip 16 (21) (2016) 4152–4162.
[12] M. Raasch, K. Rennert, T. Jahn, C. Gärtner, G. Schönfelder, O. Huber, A.E. Seiler, A.S. Mosig, An integrative microfluidically supported in vitro model of an endothelial barrier combined with cortical spheroids simulates effects of neuroinflammation in neocortex development, Biomicrofluidics 10 (4) (2016) 044102.
[13] F.R. Walter, S. Valkai, A. Kincses, A. Petneházi, T. Czeller, S. Veszelka, P. Ormos, M.A. Deli, A. Dér, A versatile lab-on-a-chip tool for modelling biological barriers, Sensors Actuators B Chem. 222 (2016) 1209–1219.
[14] J.A. Brown, V. Pensabene, Markov Da, V. Allwardt, M.D. Neely, M. Shi, C.M. Britt, O.S. Hoilett, Q. Yang, B.M. Brewer, P.C. Samson, L.J. McCawley, J.M. May, D.J. Webb, D. Li, A.B. Bowman, R.S. Reiserer, J.P. Wikswo, Recreating blood-brain barrier physiology and structure on chip: a novel neurovascular microfluidic bioreactor, Biomicrofluidics 9 (5) (2015) 054124.
[15] L.M. Griep, F. Wolbers, B. de Wagenaar, P.M. ter Braak, B.B. Weksler, I.A. Romero, P.O. Couraud, I. Vermes, A.D. Van Der Meer, A. Van Den Berg, BBB on chip: microfluidic platform to mechanically and biochemically modulate blood-brain barrier function, Biomed. Microdevices 15 (1) (2013) 145–150.
[16] P.P. Partyka, G.A. Godsey, J.R. Galie, M.C. Koscuik, N.K. Acharya, R.G. Nagele, P.A. Galie, Mechanical stress regulates transport in a compliant 3D model of the blood-brain barrier, Biomaterials 115 (2017) 30–39.
[17] A. Herland, A.D. Van Der Meer, E.A. Fitzgerald, T.E. Park, J.J. Sleeboom, D.E. Ingber, Distinct contributions of astrocytes and pericytes to neuroinflammation identified in a 3D human blood-brain barrier on a chip, PLoS One 11 (3) (2016) e0150360.
[18] G. Adriani, D. Ma, A. Pavesi, R.D. Kamm, E.L. Goh, A 3D neurovascular microfluidic

model consisting of neurons, astrocytes and cerebral endothelial cells as a blood-brain barrier, Lab Chip 17 (3) (2017) 448–459.
[19] R. Gromnicova, H.A. Davies, P. Sreekanthreddy, I.A. Romero, T. Lund, I.M. Roitt, J.B. Phillips, D.K. Male, Glucose-coated gold nanoparticles transfer across human brain endothelium and enter astrocytes in vitro, PLoS One 8 (12) (2013) e81043.
[20] P. Sreekanthreddy, R. Gromnicova, H. Davies, J. Phillips, I.A. Romero, D. Male, A three-dimensional model of the human blood-brain barrier to analyse the transport of nanoparticles and astrocyte/endothelial interactions, F1000Res. 4 (2015) 1279.
[21] N.D. Klein, K.R. Hurley, Z.V. Feng, C.L. Haynes, Dark field transmission electron microscopy as a tool for identifying inorganic nanoparticles in biological matrices, Anal. Chem. 87 (8) (2015) 4356–4362.
[22] A.M. Schrand, A.J. Schlager, L. Dai, S.M. Hussain, Preparation of cells for assessing ultrastructural localization of nanoparticles with transmission electron microscopy, Nat. Protoc. 5 (4) (2010) 744–757.
[23] T.M. Mayhew, C. Mühlfeld, D. Vanhecke, M. Ochs, A review of recent methods for efficiently quantifying immunogold and other particles using TEM sections through cells, tissues and organs, Ann. Anat. 191 (2) (2009) 153–170.
[24] M. Malatesta, Transmission electron microscopy for nanomedicine: novel applications for long-established techniques, Eur. J. Histochem. 60 (4) (2016) 2751.
[25] J.V. Georgieva, R.P. Brinkhuis, K. Stojanov, C.A. Weijers, H. Zuilhof, F.P. Rutjes, D. Hoekstra, J.C. Van Hest, I.S. Zuhorn, Peptide-mediated blood-brain barrier transport of polymersomes, Angew. Chem. Int. Ed. Eng. 51 (33) (2012) 8339–8342.
[26] K. Stojanov, J.V. Georgieva, R.P. Brinkhuis, J.C. Van Hest, F.P. Rutjes, R.A. Dierckx, E.F. De Vries, I.S. Zuhorn, In vivo biodistribution of prion- and GM1-targeted polymersomes following intravenous administration in mice, Mol. Pharm. 9 (6) (2012) 1620–1627.
[27] L.M. Van Oppen, L.K. Abdelmohsen, S.E. Van Emst-De Vries, P.L. Welzen, D.A. Wilson, J.A. Smeitink, W.J. Koopman, R. Brock, P.H. Willems, D.S. Williams, J.C. Van Hest, Biodegradable synthetic organelles demonstrate ROS shielding in human complex I deficient fibroblasts, ACS Cent. Sci. 4 (7) (2018) 917–928.
[28] P. Candela, F. Gosselet, F. Miller, V. Buee-Scherrer, G. Torpier, R. Cecchelli, L. Fenart, Physiological pathway for low-density lipoproteins across the blood-brain barrier: transcytosis through brain capillary endothelial cells in vitro, Endothelium 15 (5–6) (2008) 254–264.
[29] B. Dehouck, L. Fenart, M.P. Dehouck, A. Pierce, G. Torpier, R. Cecchelli, A new function for the LDL receptor: transcytosis of LDL across the blood-brain barrier, J. Cell Biol. 138 (4) (1997) 877–889.
[30] E.A. Biemans, L. Jäkel, R.M. De Waal, H.B. Kuiperij, M.M. Verbeek, Limitations of the hCMEC/D3 cell line as a model for Aβ clearance by the human blood-brain barrier, J. Neurosci. Res. 95 (7) (2017) 1513–1522.
[31] I.E. Allijn, W. Leong, J. Tang, A. Gianella, A.J. Mieszawska, F. Fay, G. Ma, S. Russell, C.B. Callo, R.E. Gordon, E. Korkmaz, J.A. Post, Y. Zhao, H.C. Gerritsen, A. Thran, R. Proksa, H. Daerr, G. Storm, V. Fuster, E.A. Fisher, Z.A. Fayad, W.J. Mulder, D.P. Cormode, Gold nanocrystal labeling allows low density lipoprotein imaging from the subcellular to macroscopic level, ACS Nano 7 (11) (2013) 9761–9770.